Spin-Glass Model Governs Laser Multiple Filamentation

W. Ettoumi,[1,*] J. Kasparian,[2] and J.-P. Wolf[1]
[1]Université de Genève, GAP-Biophotonics, Chemin de Pinchat 22, CH-1211 Geneva 4, Switzerland
[2]Université de Genève, GAP-Non-linear, Chemin de Pinchat 22, CH-1211 Geneva 4, Switzerland
(Received 9 March 2015; published 14 July 2015)

We show that multiple filamentation patterns in high-power laser beams can be described by means of two statistical physics concepts, namely, self-similarity of the patterns over two nested scales and nearest-neighbor interactions of classical rotators. The resulting lattice spin model perfectly reproduces the evolution of intense laser pulses as simulated by the nonlinear Schrödinger equation, shedding new light on multiple filamentation. As a side benefit, this approach drastically reduces the computing time by 2 orders of magnitude as compared to the standard simulation methods of laser filamentation.

DOI: 10.1103/PhysRevLett.115.033902 PACS numbers: 42.65.Tg, 42.65.Jx, 42.65.Sf

The nonlinear Schrödinger equation (NLSE), originally emanating from quantum mechanics, is paradigmatic of a universal equation which is widely used in a variety of fields such as nonlinear optics [1], Bose-Einstein condensates [2,3], plasma physics [4], or fluid mechanics [5]. Its analytical properties are quite well known, and exhibit features such as integrability in one dimension [6], or finite-time blow up for higher spatial dimensions [7,8].

In the field of nonlinear optics, the NLSE describes light filaments [9,10] forming in the propagation of laser pulses whose power exceeds a certain critical value. For powers much beyond the latter, the beam breaks up into many cells, each generating one filament [11–13], forming complex multiple filamentation patterns [14]. We recently showed that the formation of such patterns from an initially smooth laser beam profile defines a two-dimensional phase transition governing the geometrical structuring of the beam and the self-organization of light filaments [15]. The patterns associated to this phase transition are similar to those produced by percolation [16,17] or spin models from the statistical physics literature [18–20].

The salient features of such systems generally arise from the nearest-neighbor interactions between the underlying constituents, mainly quantum or classical spins. However, the description of multiple filamentation patterns as the result of basic interacting elements like spins was never considered until now. Laser filaments have been shown to laterally interact with their neighbors located at a distance of several millimeters in the beam profile [21–26]. This interaction is attractive if the filaments are in phase, and repulsive if they are in antiphase [27,28], because it is mediated by interference of the photon bath surrounding each filament [29–32]. However, such interactions have up to now been only considered locally. No impact on the global beam profile evolution was investigated, or even expected.

In this Letter, we derive a model for laser multiple filamentation, showing that this physical phenomenon can be understood as a consequence of self-similarity and nearest-neighbor interaction between coarse-grained light elements. This results in a description highly reminiscent of the Edwards-Anderson spin-glass model [33–36], quantitatively bridging nonlinear optics to out-of-equilibrium statistical physics.

In the following, we will first discuss the self-similarity of multiple filamentation patterns. Then, we will show that it allows us to drastically coarse grain the dynamics with minimal loss of information, provided time is adequately rescaled to account for the change in the speed of transverse information flow induced by this procedure. The resulting lattice spin model will then be validated by a direct confrontation to the results of the standard NLSE integration, showing an amazing agreement.

The starting point of our derivation is the NLSE, which, in dimensionless units, reads

$$i\partial_\eta \psi + \Delta\psi + f(|\psi|^2)\psi = 0, \tag{1}$$

where η is the propagation distance, $\Delta \equiv \partial_x^2 + \partial_y^2$ the two-dimensional transverse Laplacian, which accounts for geometrical diffraction, and the function f describes the nonlinear physical mechanisms at play, including dissipation and saturation. Although the NLSE is ubiquitous in physics, in the following we mainly focus on the case of multiple filamentation, where pattern formation is well characterized both experimentally [37] and theoretically [15]. In filamentation, ψ is the electric field envelope, and for numerical simulations it is quite common to model the nonlinearity as

$$f(|\psi|^2) = |\psi|^2 - |\psi|^{2K} + i\nu|\psi|^{2K-2}, \tag{2}$$

where the first term accounts for the Kerr self-focusing effect, and the two last ones model defocusing by free electrons as well as losses due to the K-photon ionization releasing these electrons.

Equation (1) features a linear instability, called the modulational instability, with spectacular experimental consequences ranging from the emergence of solitons in Bose-Einstein condensates [38,39] to the formation of multiple filamentation patterns [40–43] in large high-power laser beams. The growth rate γ of this instability can be obtained analytically. For a plane wave steady state $\psi_0 e^{i\lambda\eta}$, writing $k_\perp$ the spatial transverse wave vector of the perturbation leads to [22]

$$\gamma = k_\perp \sqrt{2\psi_0^2 f'(\psi_0^2) - k_\perp^2}. \tag{3}$$

Figure 1 displays the resulting patterns in the case of laser propagation in air by solving numerically Eq. (1). The initial condition is taken as a fourth-order super-Gaussian of 5 cm diameter, holding 50 TW at a wavelength of 800 nm. The relationship between the dimensionless units and the real physical parameters is given in the Supplemental Material [44]. The modulational instability, seeded by the initial beam noise [Fig. 1(a)], triggers the emergence of mesoscopic structures [Fig. 1(b)] which are later amplified [Fig. 1(c)] by the nonlinearities in Eq. (2). Furthermore, Fig. 1(d) displays a close-up of the center of the beam after 7 m of propagation. The patterns are quite similar at both scales. In particular, they share the following common features: (i) local maxima attracting intensity, depleting the energy around them, (ii) strings of intermediate intensity connecting these local maxima, (iii) regions of weaker intensity (photon bath) around them, (iv) lateral interactions between the maxima structures, and (v) the overall shrinking of the whole pattern towards a structure with the lower length scale. Similar patterns can therefore be observed on two spatial scales, 2 orders of magnitude apart in size.

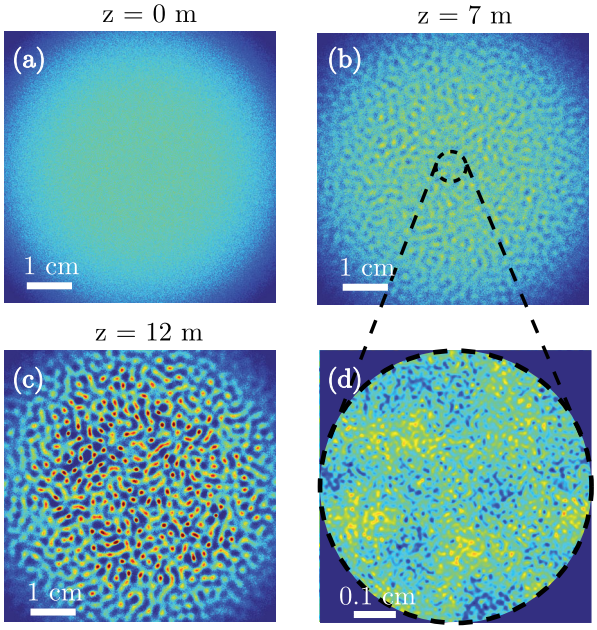

FIG. 1 (color online). (a), (b), and (c) Evolution of an initially perturbed flat top laser profile of 50 TW at 800 nm, with 5 cm waist. The modulational instability seeds the emergence of a pattern, which self-sustains when nonlinear effects come into action. (d) Magnification of a central zone showing self-similarity.

Beyond the visual aspect, the self-similarity can be quantitatively evidenced by investigating the structure factor S_ϕ of the laser fluence $A \equiv |\psi|^2$, defined by

$$S_\phi(\mathbf{k}, \eta) = \langle |\hat{A}(\mathbf{k}, \eta)|^2 \rangle, \tag{4}$$

where the hat denotes the Fourier transform, and the brackets an ensemble average. Figure 2(a) displays three spectra corresponding to two stages of the evolution of the laser beam. Starting from a flat transverse spectrum describing the various length scales of the initial profile modulated with a white noise, the modulational instability seeds the emergence of the characteristic patterns at stake here. The peaks on the spectrums after 7 and 12 m propagation depict the aforementioned multiple scales constituting the self-similarity.

We define the characteristic length ξ of the patterns using the structure factor as

$$\xi(\eta) = \frac{\int S_\phi(k, \eta) dk}{\int k S_\phi(k, \eta) dk}. \tag{5}$$

During the propagation, ξ first increases from the initial noise correlation length until a maximum length attained at the percolation threshold [15] [Fig. 2(b)]. This increase differs from the monotonic decay of the correlation length that is obtained with thresholded, two-color images [15]. At further propagation distances, the fluence clusters either vanish because of dissipation, or get squeezed in size because of the energy flux towards their center, resulting in a decrease of ξ.

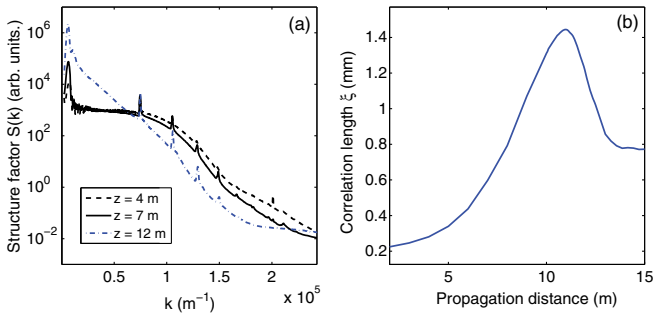

FIG. 2 (color online). (a) Structure factor $S_\phi(k)$ calculated after 4 m (representative of the initial conditions), 7 m, and 12 m of propagation. Note that we have suppressed the zero peak for clarity reasons. (b) Evolution of the correlation length ξ [Eq. (5)] for a 800 nm, 50 TW beam of 5 cm waist.

The images shown on Fig. 1 are reminiscent of many models studied by the statistical mechanics community. One can note a striking resemblance with coarsening phenomena [48,49]: here, the transverse low and high intensity regions can be seen as two different phases of a generic model evolving under Ginzburg-Landau dynamics [50].

This behavior is generally well reproduced by simple spin models with proper time dynamics, and we shall now derive a lattice spin model (LSM) of filamentation, based on the previous observations. The patterns' topology we aim at reproducing is mainly due to the combined effects of modulational instability and Kerr nonlinearity. We therefore truncate f [Eq. (2)] to its cubic contribution in ψ.

The patterns shown in Fig. 1 strongly suggest modeling the electric field by a superposition of narrow, Gaussian-like, elementary wavelets. We chose their spatial extensions comparable to the lowest-order structure in the beam, i.e., 10 μm. Therefore, the field can be expanded as $\psi(\mathbf{r},\eta)=\sum_n A_n(\mathbf{r},\eta)e^{i\phi_n(\mathbf{r},\eta)}$.

The universality class unveiled in [15] suggests that the behavior of a lattice model close to criticality should be independent from the microscopic detail, and *a fortiori* from the lattice geometry. Hence, we define the set of $\{\mathbf{r_n}\}$ as a square lattice. Projecting Eq. (1) on each $e^{i\phi_n}$ and identifying real and imaginary parts leads to

$$\partial_\eta A_n = -2\boldsymbol{\nabla}A_n\cdot\boldsymbol{\nabla}\phi_n - A_n\Delta\phi_n, \tag{6}$$

$$A_n\partial_\eta\phi_n = \Delta A_n - A_n|\boldsymbol{\nabla}\phi_n|^2 + A_n\sum_{\ell,m}A_\ell A_m\cos(\phi_\ell-\phi_m). \tag{7}$$

By definition, A_n displays a maximum at $\mathbf{r}=\mathbf{r_n}$. Considering that the phase ϕ_n is strongly impacted by the B integral [10], hence by the amplitude A_n, we assume that it also has an extremum at the same location. Therefore, Eqs. (6) and (7) can be simplified by canceling every first spatial derivative. As detailed in the Supplemental Materal [44], the spatial self-similarity allows us to derive a lattice model in which each square lattice site n of area δ^2 holds two observables, A_n and ϕ_n, being the respective averages of the amplitude and phase over the lattice sites:

$$\dot{A}_n = -\kappa[\phi_n]A_n, \tag{8}$$

$$\dot{\phi}_n = \frac{\kappa[A_n]}{A_n} + A_n^2 + A_n\sum_{\langle\ell\rangle_n}A_\ell\cos(\phi_n-\phi_\ell). \tag{9}$$

The dots in Eqs. (8) and (9) refer to a "time" derivative, which will reproduce the propagation dynamics of the original NLSE, and where κ is the discretized Laplacian over the four nearest neighbors. For a site (i,j), it reads $\kappa[\phi_{i,j}]=(1/\delta^2)(-4\phi_{i,j}+\phi_{i+1,j}+\phi_{i-1,j}+\phi_{i,j+1}+\phi_{i,j-1})$.

Equations (8) and (9) are the main result of this Letter. Each lattice site can be seen as an individual classical rotator, described by two observables, A and ϕ, which are its length and angle, respectively. These rotators evolve under nearest-neighbor interactions, arising from both the discretized Laplacians and the last term of Eq. (9), accounting for the coarse-grained interference phenomenon. For instance, if two lattice neighbors share a common optical phase, their amplitudes will constructively interfere, mimicking the situation in which two filaments attract each other, and eventually merge. Conversely, if these two neighbors feature a relative phase shift of π, a destructive interference will decrease their amplitudes and eject their energy towards sites further away, as reported experimentally [28].

The interaction term $J_{n\ell}\equiv\cos(\phi_n-\phi_\ell)$ is typical of the spin-glass model, e.g., the soft-spin version of the Edwards-Anderson model [33–35,51], characterized by the interaction Hamiltonian between spins σ_i, $\mathcal{H}=-\sum_{\langle i,j\rangle}J_{ij}\sigma_i\sigma_j$ and evolving under a phenomenological Langevin equation,

$$\dot{\sigma}_i = -\beta\frac{\delta\mathcal{H}}{\delta\sigma_i}+\xi_i = \beta\sum_{\langle j\rangle_i}J_{ij}\sigma_j+\xi_i, \tag{10}$$

β being the inverse temperature and ξ_i a Gaussian random variable.

As a test for the relevance of the presented LSM, we will now compare its pattern predictions with the results obtained by integrating the NLSE using a standard split-step Fourier method (SSFM). As an initial condition, we use an already slightly propagated beam (by 4 m) with the same properties as in Fig. 1. In general, one could estimate the coarse-graining length δ as being the inverse of the wavelength maximizing the linear growth rate γ, since clusters of such a size are expected to emerge quicker than others. Doing so with an initial condition as presented here yields $\delta=924$ μm, in good agreement with the actual physical range as the size of the photon bath surrounding a single filament is typically between 500 and 1000 μm. Practically speaking, starting from the field ψ, we define the spins (A_n,ϕ_n) as

$$A_n = \left(\frac{1}{\delta^2}\iint_{\Sigma_n}|\psi(\mathbf{r_n}+\mathbf{r}')|^2d^2\mathbf{r}'\right)^{1/2}, \tag{11}$$

$$\phi_n = \frac{1}{\delta^2}\iint_{\Sigma_n}\phi(\mathbf{r_n}+\mathbf{r}')d^2\mathbf{r}', \tag{12}$$

where Σ_n stands for the lattice cell n of area δ^2. Note that it is important to average the fluence $|\psi|^2$, and then only take the square root instead of directly averaging the field ψ.

This way, Eq. (11) ensures the conservation of the photon number $P_0 = \sum_n \delta^2 A_n^2$.

A direct integration of Eqs. (8) and (9) yields a very good qualitative agreement with the reference NLSE patterns computed with the SSFM. However, the smallest coarse-grained length scales of order δ (typically millimetric) behave within the same time scale in the LSM as their much smaller counterparts of a hundred micrometers in the NLSE hereafter denoted by ℓ_c. As a consequence, a pattern arising after a few meters would be predicted after only a few centimeters by the LSM.

However, a linear stability analysis shows that the LSM exhibits the same growth rate given by Eq. (3) as the NLSE, which is remarkable. Based on this result, we devised a strategy detailed in the Supplemental Material [44] in order to recover the proper dynamics, introducing a rescaled time variable τ reading

$$\tau = \eta \sqrt{\frac{\ell_c}{\delta}}. \tag{13}$$

This time renormalization therefore ensures that the LSM correctly reproduces the speed of the transverse diffusion of information.

In our case, we considered a coarse-graining length $\delta = 732$ μm, i.e., 40 pixels in our reference NLSE numerical resolution. Since we smoothed our initial random noise over a length of 4 pixels, we set the small-scale cutoff length $\ell_c = \delta/10 = 73.2$ μm. From Eq. (13), we deduce that the time renormalization factor is equal to 0.32. Again, this factor lower than unity translates the fact that the coarse-graining causes the LSM to act on the patterns much quicker than the NLSE does, since the former is an upscaled version of the latter.

We first set a flat initial phase, namely, a real initial ψ. Figures 3(a)–3(e) compare the fluence pattern obtained from both the LSM and the NLSE after approximately 9 m of free propagation. Despite the apparent lack of information in the initial condition (at 4 m), the LSM remarkably reproduces the final reference NLSE pattern, showing that the interpretation of multiple filamentation in terms of interacting spins yields quantitative predictions. This is very remarkable as filamentation is generally considered as a local phenomenon requiring a high spatial resolution in order to capture its salient features.

To check the fidelity of the phase evolution in a "worst-case scenario," we also considered initial abrupt phase jumps from zero to $-\pi/2$ [Fig. 3(i)]. This case was chosen because of the difficulty of stimulating fields with steep gradients, which result in strong diffraction and instabilities that can only be resolved at extremely high resolutions. A coarse-grained model intrinsically cannot capture such features, making this situation a robustness check of the LSM.

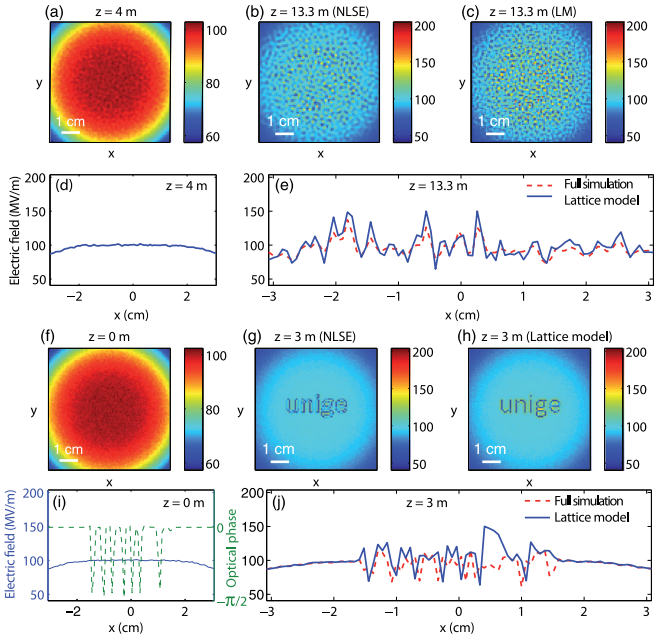

FIG. 3 (color online). Comparison between the lattice spin model and the coarse-grained result of the NLSE simulation using the SSFM. (a)–(e), flat initial phase; (f)–(j), worst-case scenario with $\pi/2$ phase jumps. (a),(f) Initial condition for the LSM, originating from a full resolution SSFM integration, (b),(g) LSM output; (c),(h) NLSE output using SSFM; (e),(j) horizontal cuts across the model outputs.

We modulated the aforementioned amplitude pattern by a phase mask displaying the word "unige." Figure 3 shows a remarkable agreement after 3 m of free propagation, despite a glitch on the reproduction of the letter "g."

Moreover, these results are not tributary to a fine-tuned choice of the coarse-graining length δ. One can freely choose it in the aforementioned physically acceptable range and still obtain reasonable results, whereas a decrease of resolution in the SSFM method rapidly leads to erroneous simulations.

These two cases highlight the relevance and the quantitative accuracy of the LSM. For smooth initial phases, the relative error on intensity stays below 10%. The importance of nearest-neighbor interaction was demonstrated by switching off the corresponding term in Eq. (9). The beam then keeps a smooth shape very different from what is observed in both experiments and NLSE simulations.

It is quite straightforward to derive richer lattice models encompassing more phenomena, such as saturation mechanisms, plasma generation [see Eq. (2)], or even air turbulence. This would simply require expanding the additional physical model on the wavelet basis, and then simplify all the remaining terms by keeping in mind the nearest-neighbor picture.

As a conclusion, we took advantage of the self-similarity of multiple filamentation patterns to introduce the description of laser multiple filamentation as a lattice spin model

with glassylike dynamics. The numerical benchmarks showed an excellent agreement with the full calculations, demonstrating the robustness of such a novel interpretation, that can also be related to the recent observation of a percolationlike phase transition in such a system [15]. Furthermore, as a consequence of the coarse-grained description, the small lattice sizes at play allow computing times faster by 2 orders of magnitude as compared to standard SSFM calculations. Such a speedup opens the way to statistical studies of, e.g., beam propagation through turbulence or explicit inversion of nonlinear Lidar measurements [52–54] of atmospheric trace constituents.

In a wider scope, our approach only relies on the structure of the NLSE, not on a particular nonlinearity (i.e., a particular function f) nor its application to a specific physical system. Therefore, it can be generalized to other fields of physics described by the NLSE, where such self-similarity could also be observed and exploited [55–57].

We wish to warmly thank an anonymous referee for very valuable comments and suggestions. We gratefully acknowledge fruitful discussions with T. Giamarchi, M. Brunetti, and S. Hermelin. We acknowledge financial support from the European Research Council Advanced Grant "Filatmo" and the Swiss National Science Foundation (Grant No. 200021-155970).

*wahb.ettoumi@unige.ch

[1] M. Gedalin, T. C. Scott, and Y. B. Band, Phys. Rev. Lett. **78**, 448 (1997).
[2] P. A. Ruprecht, M. J. Holland, K. Burnett, and M. Edwards, Phys. Rev. A **51**, 4704 (1995).
[3] C. C. Bradley, C. A. Sackett, J. J. Tollett, and R. G. Hulet, Phys. Rev. Lett. **75**, 1687 (1995).
[4] K. Mio, T. Ogino, K. Minami, and S. Takeda, J. Phys. Soc. Jpn. **41**, 265 (1976).
[5] K. B. Dysthe, Proc. R. Soc. A **369**, 105 (1979).
[6] H. Chen, Y. Lee, and C. Liu, Phys. Scr. **20**, 490 (1979).
[7] R. T. Glassey, J. Math. Phys. (N.Y.) **18**, 1794 (1977).
[8] G. Fibich and G. Papanicolaou, SIAM J. Appl. Math. **60**, 183 (1999).
[9] S. L. Chin, S. A. Hosseini, W. Liu, Q. Luo, F. Théberge, N. Aközbek, A. Becker, V. P. Kandidov, O. G. Kosareva, and H. Schröder, Can. J. Phys. **83**, 863 (2005).
[10] A. Couairon and A. Mysyrowicz, Phys. Rep. **441**, 47 (2007).
[11] A. J. Campillo, S. L. Shapiro, and B. R. Suydam, Appl. Phys. Lett. **23**, 628 (1973).
[12] G. Méjean, J. Kasparian, J. Yu, E. Salmon, S. Frey, J.-P. Wolf, S. Skupin, A. Vinçotte, R. Nuter, S. Champeaux, and L. Bergé, Phys. Rev. E **72**, 026611 (2005).
[13] P. Béjot *et al.*, Appl. Phys. Lett. **90**, 151106 (2007).
[14] S. Henin, Y. Petit, J. Kasparian, J.-P. Wolf, A. Jochmann, S. D. Kraft, S. Bock, U. Schramm, R. Sauerbrey, W. M. Nakaema, K. Stelmaszczyk, P. Rohwetter, L. Wöste, C.-L. Soulez, S. Mauger, L. Bergé, and S. Skupin, Appl. Phys. B **100**, 77 (2010).
[15] W. Ettoumi, J. Kasparian, and J.-P. Wolf, Phys. Rev. Lett. **114**, 063903 (2015).
[16] K. Golden, S. Ackley, and V. Lytle, Science **282**, 2238 (1998).
[17] D. Stauffer, Phys. Rep. **54**, 1 (1979).
[18] J. Marro and R. Dickman, *Nonequilibrium Phase Transitions in Lattice Models* (Cambridge University Press, Cambridge, 2005).
[19] J. M. Kosterlitz and D. J. Thouless, J. Phys. C **6**, 1181 (1973).
[20] T. M. Rogers and R. C. Desai, Phys. Rev. B **39**, 11956 (1989).
[21] C. Ren, R. G. Hemker, R. A. Fonseca, B. J. Duda, and W. B. Mori, Phys. Rev. Lett. **85**, 2124 (2000).
[22] L. Bergé, C. Gouédard, J. Schjodt-Eriksen, and H. Ward, Physica (Amsterdam) **176D**, 181 (2003).
[23] S. A. Hosseini, Q. Luo, B. Ferland, W. Liu, S. L. Chin, O. G. Kosareva, N. A. Panov, N. Aközbek, and V. P. Kandidov, Phys. Rev. A **70**, 033802 (2004).
[24] Y. Y. Ma, X. Lu, T. T. Xi, Q. H. Gong, and J. Zhang, Appl. Phys. B **93**, 463 (2008).
[25] E. D'Asaro, S. Heidari-Bateni, A. Pasquazi, G. Assanto, J. Gonzalo, J. Solis, and C. N. Afonso, Opt. Express **17**, 17150 (2009).
[26] L. Bergé, M. R. Schmidt, J. J. Rasmussen, P. L. Christiansen, and K. Ø. Rasmussen, J. Opt. Soc. Am. B **14**, 2550 (1997).
[27] T. T. Xi, X. Lu, and J. Zhang, Phys. Rev. Lett. **96**, 025003 (2006).
[28] B. Shim, S. E. Schrauth, C. J. Hensley, L. T. Vuong, P. Hui, A. A. Ishaaya, and A. L. Gaeta, Phys. Rev. A **81**, 061803 (2010).
[29] W. Liu, F. Théberge, E. Arévalo, J.-F. Gravel, A. Becker, and S. L. Chin, Opt. Lett. **30**, 2602 (2005).
[30] F. Courvoisier, V. Boutou, J. Kasparian, E. Salmon, G. Méjean, J. Yu, and J.-P. Wolf, Appl. Phys. Lett. **83**, 213 (2003).
[31] M. Kolesik and J. V. Moloney, Opt. Lett. **29**, 590 (2004).
[32] S. Skupin, L. Bergé, U. Peschel, and F. Lederer, Phys. Rev. Lett. **93**, 023901 (2004).
[33] S. F. Edwards and P. W. Anderson, J. Phys. F **5**, 965 (1975).
[34] J. De Almeida and D. J. Thouless, J. Phys. A **11**, 983 (1978).
[35] L. F. Cugliandolo and J. Kurchan, Phys. Rev. Lett. **71**, 173 (1993).
[36] L. Cugliandolo and J. Kurchan, J. Phys. A **27**, 5749 (1994).
[37] S. Henin, Y. Petit, J. Kasparian, J.-P. Wolf, A. Jochmann, S. D. Kraft, S. Bock, U. Schramm, R. Sauerbrey, W. M. Nakaema, K. Stelmaszczyk, P. Rohwetter, L. Wöste, C.-L. Soulez, S. Mauger, L. Bergé, and S. Skupin, Appl. Phys. B **100**, 77 (2010).
[38] L. D. Carr and J. Brand, Phys. Rev. Lett. **92**, 040401 (2004).
[39] J. Denschlag, J. Simsarian, D. Feder, C. W. Clark, L. Collins, J. Cubizolles, L. Deng, E. Hagley, K. Helmerson, W. Reinhardt *et al.*, Science **287**, 97 (2000).
[40] V. P. Kandidov, O. G. Kosareva, M. P. Tamarov, A. Brodeur, and S. L. Chin, Quantum Electron. **29**, 911 (1999).
[41] M. Mlejnek, M. Kolesik, J. V. Moloney, and E. M. Wright, Phys. Rev. Lett. **83**, 2938 (1999).
[42] S. A. Hosseini, J. Yu, Q. Luo, and S. L. Chin, Appl. Phys. B **79**, 519 (2004).

[43] C. Ren, R. G. Hemker, R. A. Fonseca, B. J. Duda, and W. B. Mori, Phys. Rev. Lett. **85**, 2124 (2000).
[44] See Supplemental Material at http://link.aps.org/supplemental/10.1103/PhysRevLett.115.033902, which includes Refs. [45–47], for details about the lattice spin model derivation and time renormalization procedure.
[45] S. Skupin, L. Bergé, U. Peschel, F. Lederer, G. Méjean, J. Yu, J. Kasparian, E. Salmon, J. P. Wolf, M. Rodriguez, L. Wöste, R. Bourayou, and R. Sauerbrey, Phys. Rev. E **70**, 046602 (2004).
[46] H. Sakaguchi, S. Shinomoto, and Y. Kuramoto, Prog. Theor. Phys. **77**, 1005 (1987).
[47] J. A. Acebrón, L. L. Bonilla, C. J. P. Vicente, F. Ritort, and R. Spigler, Rev. Mod. Phys. **77**, 137 (2005).
[48] A. J. Bray, Adv. Phys. **43**, 357 (1994).
[49] A. Bray, B. Derrida, and C. Godreche, Eur. Phys. Lett. **27**, 175 (1994).
[50] L. Berthier, J.-L. Barrat, and J. Kurchan, Eur. Phys. J. B **11**, 635 (1999).
[51] H. Sompolinsky and A. Zippelius, Phys. Rev. B **25**, 6860 (1982).
[52] P. R. Hemmer, R. B. Miles, P. Polynkin, T. Siebert, A. V. Sokolov, P. Sprangle, and M. O. Scully, Proc. Natl. Acad. Sci. U.S.A. **108**, 3130 (2011).
[53] A. Natan, J. M. Levitt, L. Graham, O. Katz, and Y. Silberberg, Appl. Phys. Lett. **100**, 051111 (2012).
[54] M. T. Bremer and M. Dantus, Appl. Phys. Lett. **103**, 061119 (2013).
[55] W. Bao, D. Jaksch, and P. A. Markowich, J. Comp. Physiol. **187**, 318 (2003).
[56] C. Fort, L. Fallani, V. Guarrera, J. E. Lye, M. Modugno, D. S. Wiersma, and M. Inguscio, Phys. Rev. Lett. **95**, 170410 (2005).
[57] M. Modugno, Phys. Rev. A **73**, 013606 (2006).